

Supporting Information for:

Experimental and Theoretical Study of a Cadmium Coordination Polymer based on Aminonicotinate with Second-Timescale Blue/Green Photoluminescent Emission

Jose M. Seco,^a Antonio Rodríguez-Diéguez,^b Daniel Padro,^c Jose A. García,^d Jesus M. Ugalde,^e Eider San Sebastian,^{*a} and Javier Cepeda^{*a,c}

^a Applied Chemistry Department, Chemistry Faculty, University of the Basque Country (UPV/EHU), 20080 Donostia, Spain. ^b Inorganic Chemistry Department, Chemistry Faculty, University of Granada, 18071 Granada, Spain. ^c Nuclear Magnetic Resonance Platform, CIC BiomaGUNE, 20080 Donostia, Spain. ^d Applied Physics Department, Science and Technology Faculty, University of the Basque Country, UPV/EHU, 48940 Bilbao, Spain. ^e Kimika Fakultatea, Euskal Herriko Unibertsitatea (UPV/EHU) and Donostia International Physics Center (DIPC), P.K. 1072, 20080 Donostia, Euskadi, Spain.

Contents:

- S1. Materials and measurements.
- S2. Synthesis of **1**.
- S3. Powder X-ray Data Collection and Analysis.
- S4. Dispersion-corrected DFT optimization of structure.
- S5. Photoluminescence measurements.
- S6. Thermogravimetric analysis.
- S7. FT-IR spectroscopy.
- S8. Lifetime measurements.
- S9. TD-DFT computational details.
- S10. Calculation of the lowest-lying triplet state (T_1).
- S11. Time-resolved emission spectra.
- S12. References.

S1. Materials and Measurements.

All chemicals were of reagent grade and were employed as commercially obtained. Thermal analysis (TG/DTA) was performed on a TA Instruments SDT 2960 thermal analyzer from room temperature up to 800 °C in a synthetic air atmosphere (79% N₂ / 21% O₂) with a heating rate of 5 °C/min. Elemental analyses (C, H, and N) were performed on a Fisons Instruments EA-1008 analyser. Metal content was determined by inductively coupled plasma (ICP-AES) analysis with a Horiba Yobin Yvon Activa spectrometer. The FTIR spectrum (KBr pellets) was recorded on a ThermoNicolet IR 200 spectrometer in the 4000–400 cm⁻¹ spectral region. Density of the compound was performed by means of the flotation method, employing a small fragment of a pressed pellet of the compound.

S2. Synthesis of 1.

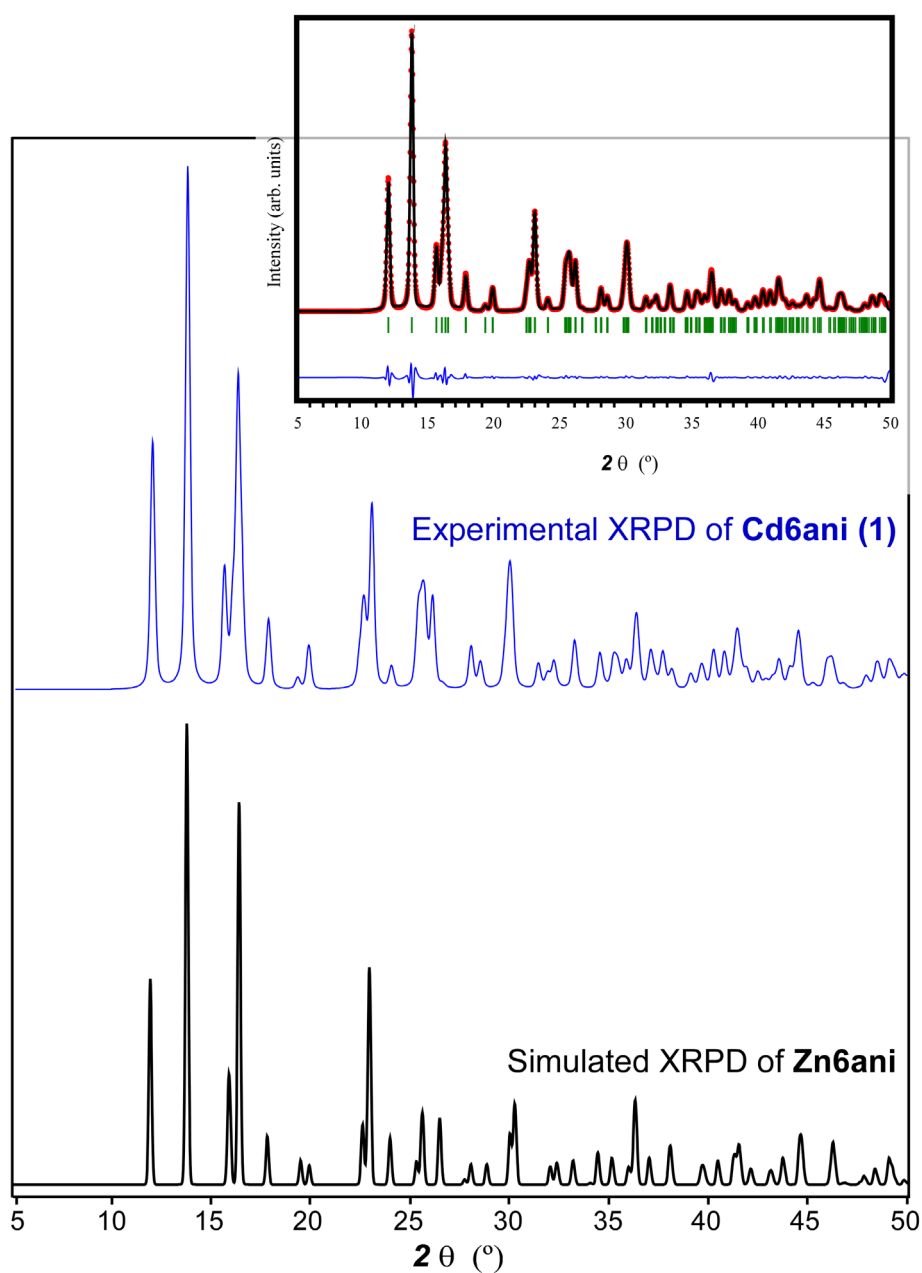
5 mL of an aqueous solution containing 0.3 mmol of Cd(NO₃)₂·4H₂O (0.1542 g) were added dropwise over an aqueous/methanol (20 mL, 1:1) solution of 0.6 mmol of H6ani (0.0828 g) under continuous stirring at 70 °C. Then, 1 mL of triethylamine (>98%) was added to the reaction mixture so that the final pH of the solution was 6.5 and a white precipitate corresponding to compound **1** was obtained. Then, the suspension was cooled down and the precipitate filtered off and washed several times with water and methanol. Compound **1** has the [Cd(μ-6ani)₂]_n formula according to elemental and thermogravimetric analyses. Elemental analysis for C₁₂H₁₀CdN₄O₄ (386.64 g mol⁻¹). Calcd.: C, 37.28; H, 2.61; Cd, 29.07; N, 14.41. Found: C, 37.14; H, 2.68; Cd, 29.25; N, 14.18.

S3. Powder X-ray Data Collection.

X-ray powder diffraction (XRPD) pattern was collected on a Phillips X'PERT powder diffractometer with Cu-Kα radiation (λ = 1.54060 Å) over the 5 < 2θ < 50° range with a step size of 0.026° and an acquisition time of 5 s per step at 25 °C. A fixed divergence slit was employed for the experiment. Indexation of the diffraction profile was made by means of the FULLPROF program (pattern-matching analysis) on the basis of the space group and the cell parameters found for the isostructural Zn6ani compound.ⁱ Details of the refinement and crystallographic data are summarized in Table S1 and Figure S1.

Table S1. Crystallographic data and structure refinement details of compound **1**.

	1		1
Empirical formula	C ₁₂ H ₁₀ CdN ₄ O ₄	Z	4
Formula weight	386.64	ρ (g cm ⁻³) (calcd. / exp.)	1.76 / 1.77(1)
Crystal system	Tetragonal	Chi ²	1.24
Space group	<i>P4₃2₁2</i>	Final R indices	
<i>a</i> (Å) (exp./DFT-D)	7.971(6) / 8.2261	R _F	1.15
<i>b</i> (Å) (exp./DFT-D)	7.971(6) / 8.2261	R _B	1.07
<i>c</i> (Å) (exp./DFT-D)	22.933(4) / 23.1391	R _P	3.61
V (Å ³) (exp./DFT-D)	1456.8(7) / 1565.8		

**Figure S1.** Comparison of experimental diffractogram of **1** and that simulated of Zn6ani compound. Inset: Full profile pat-tern-matching analysis of **1**.

S4. Dispersion corrected periodic DFT optimization of 1.

Dispersion-corrected density-functional theory calculations with periodic boundary conditions (PBC) were performed using the code SIESTA,ⁱⁱ which uses atom centered basis functions that are particularly efficient for total energy studies of very low density materials with very large unit cells. This methodology has proved to be efficient in addressing the energetics and structures of hybrid compounds.ⁱⁱⁱ Periodic DFT calculations were carried out using the PBE exchange correlation functional within the GGA approximation.^{iv} Energies of all structures in their primitive cells or unit cells were minimized by geometry optimization at constant pressure using the Broyden scheme, where both cell parameters and atomic coordinates were relaxed. No symmetry was imposed on the structure in the calculation and so the cell may relax to alternative Bravais lattice types. Double zeta plus polarization basis sets were used throughout. The hydrogen pseudopotential and basis were taken from the SIESTA database.^v In each case, the geometry was relaxed until the residual forces were smaller than $0.015 \text{ eV \AA}^{-1}$, with a stress tolerance less than 1 GPa. The Hartree and exchange–correlation potentials were evaluated using a real-space mesh with a kinetic energy cutoff of 200Ry, while the Brillouin zone was sampled only at the G point (which is reasonable given these materials are insulators with a minimum cell parameter of 9.7 \AA and a maximum of $> 32 \text{ \AA}$). Coordinates for all geometry optimized structures are given in the form of a CIF file. Correctness of the optimization is confirmed when compared the unit cell parameters and PXRD diffractograms (Figure S2) with those experimentally estimated, finding very slight deviations as in previous works.^{vi} Tables S2, S3, and S4 provide the most significant structural data.

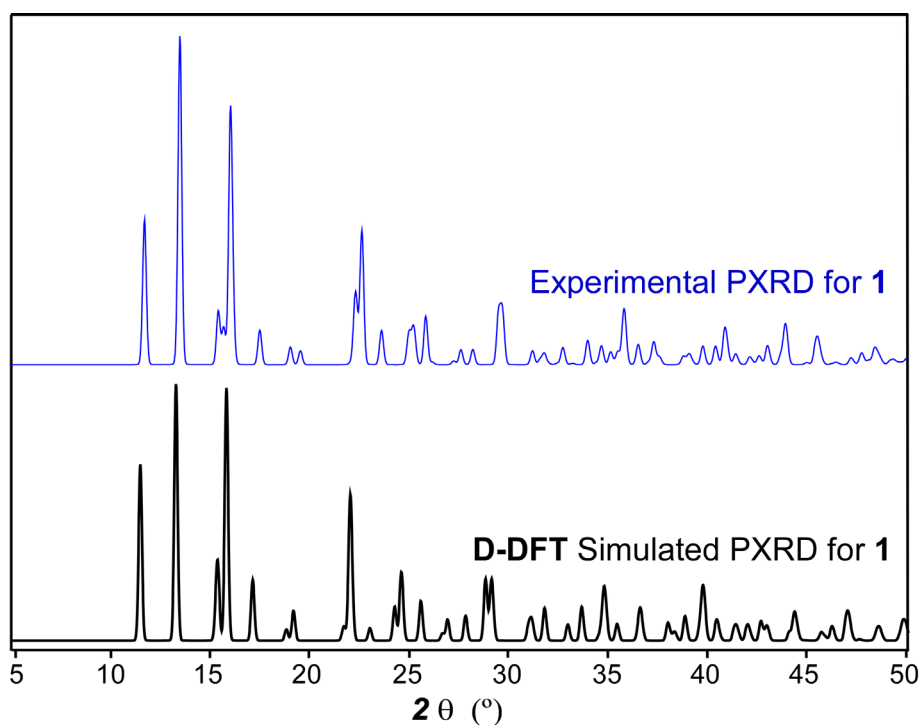


Figure S2. Comparison of experimental diffractogram of **1** and that simulated from D-DFT optimised structure of **1**.

Table S2. Selected bond lengths for compound **1**.^a

Cd1–N1	2.329	Cd1–O1(iii)	2.243
Cd1–N1(i)	2.329	Cd1–O2(ii)	2.638
Cd1–O1(ii)	2.243	Cd1–O2(iii)	2.638

[a] Symmetries: (i) $-y + 1, -x + 1, -z + 3/2$; (ii) $-y + 2, -x + 1, -z + 3/2$; (iii) $x, y - 1, z$.

Table S3. Structural parameters (Å, °) of hydrogen bonds (Å, °) in compound **1**.^a

$D-H\cdots A^b$	$D-H$	$H\cdots A$	$D\cdots A$	$D-H\cdots A$
N8–H81 \cdots O1(iii)	1.03	1.94	2.943	165.2
N8–H82 \cdots O2(iv)	1.02	2.37	3.096	127.4

^a Symmetry codes: (iv) $-y + 3/2, x - 1/2, z - 1/4$. ^b D: donor. A: acceptor.

Table S4. Structural parameters (Å, °) of π - π interactions of compound **1**.^a

Ring \cdots Ring ^b	α	DC	β	DZ	Dist.
1A–1A(v)	35.90	4.421	39.29	4.40	3.63–4.03
1A–1A(vi)	35.90	4.421	4.93	3.42	3.63–4.03

[a] Symmetry: (v) $x - 1/2, -y + 3/2, -z + 5/4$; (vi) $x + 1/2, -y + 3/2, -z + 5/4$. α : dihedral angle between mean planes of the rings (°), DC: distance between ring centroids (Å), β : angle between DC vector and normal to plane(I) (°), DZ: perpendicular distance of the centroids of ring(I) on plane of ring(II) (Å), Dist.: shorter distances between non-hydrogen atoms of rings (I) and (II). [b] Rings: **1A**: N1, C2, C3, C4, C5, C6.

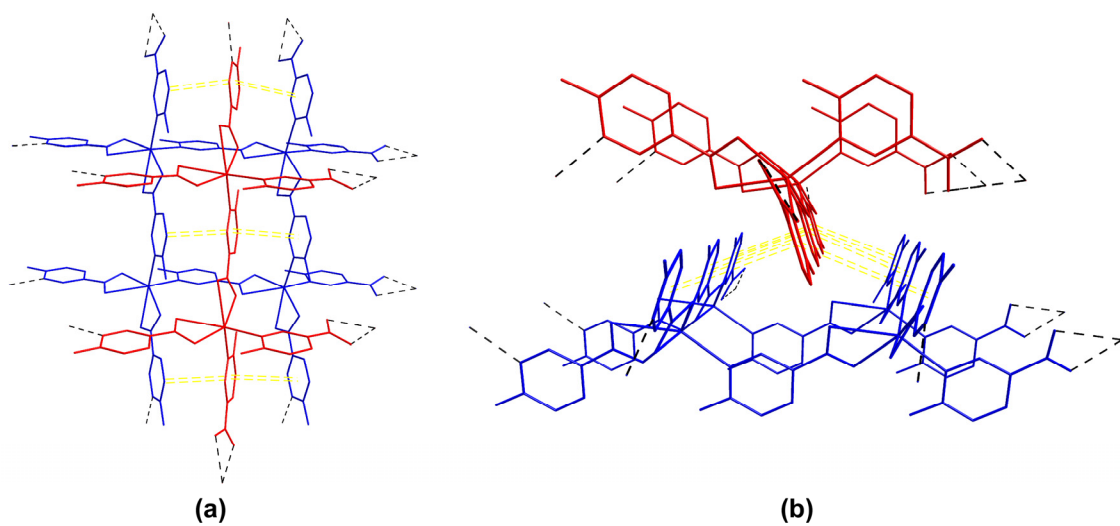


Figure S3. View of the packing of **1** showing π - π interactions between layers along: **(a)** crystallographic *b* axis and **(b)** *c* axis.

S5. Photoluminescence measurements.

Lifetime, Time Resolved Emission Spectroscopy (TRES) and steady state photoluminescence (PL) were measured on polycrystalline samples from 10 K to room temperature using a closed cycle helium cryostat enclosed in an Edinburgh Instruments FLS920 spectrometer. For steady state measurements an IK3552R-G HeCd continuous laser (325 nm) and a Müller-Elektronik-Optik SVX1450 Xe lamp were used as excitation source. Microphotoluminescence photographs were obtained at room temperature in a micro-PL system included in an Olympus optical microscope illuminated with a HeCd laser or a Hg lamp.

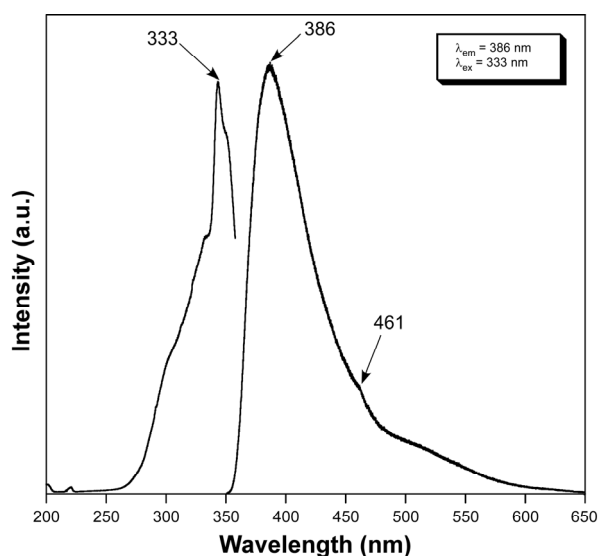


Figure S4. Excitation and emission spectra of the H6ani ligand at 10 K.

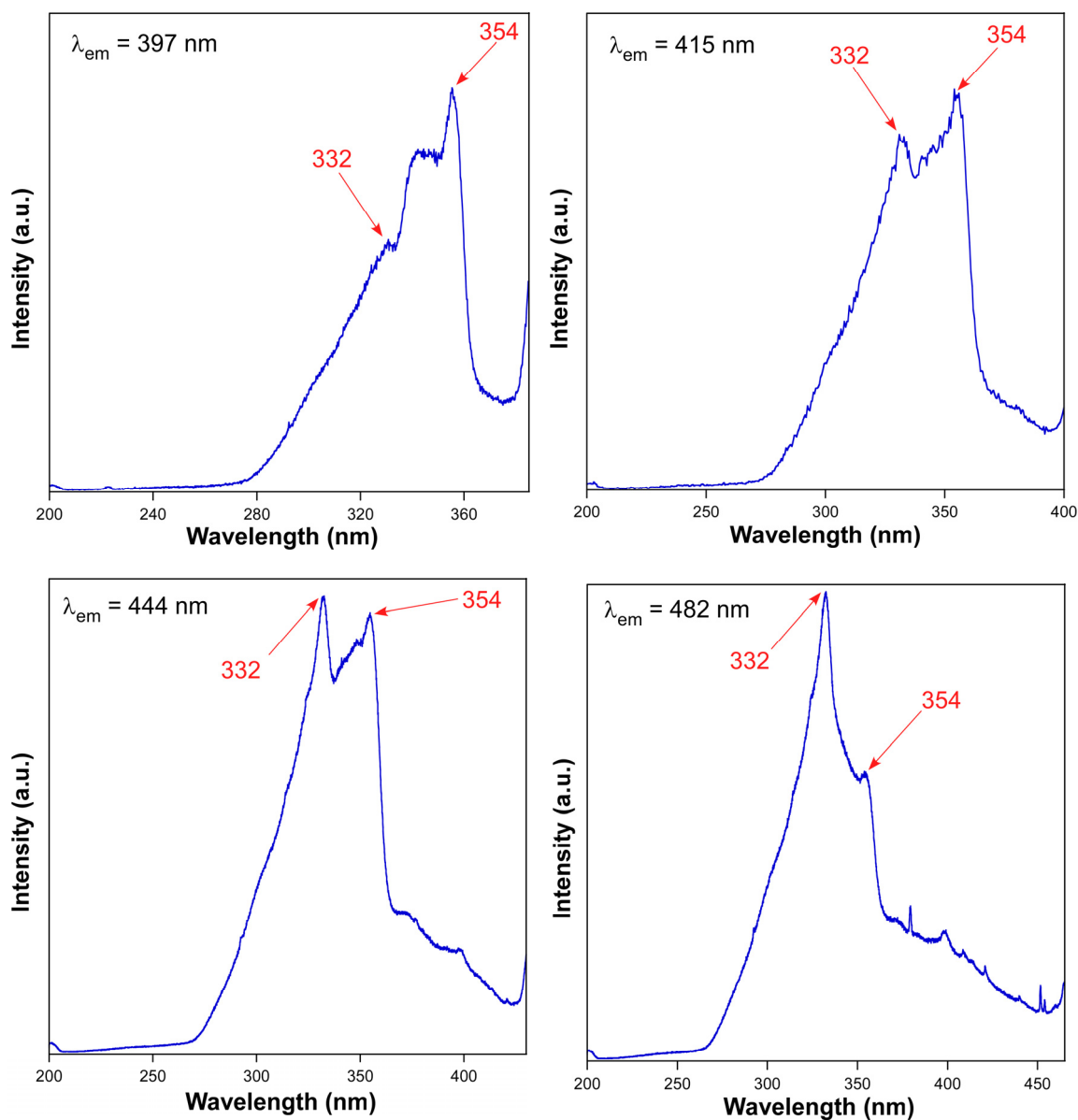


Figure S5. Evolution of the intensity of the two main excitation lines spectra of **1** monitored at different emission wavelengths.

S6. Thermogravimetric Analysis.

A plateau in the TG curve from room temperature up to 410 °C is observed in good agreement with the lack of solvent molecules in the crystal structure of compound **1**. This fact, together with the absence of DTA peaks stands for the robustness of its crystal building as a result of the strong supramolecular interactions among the Cd-6ani layers in the three-dimensional packing. Above 410 °C, compound **1** experiments several exothermic processes as a consequence of the decomposition of the organic part, leading to CdO as a final residue (calc. 32.45; 33.29%).

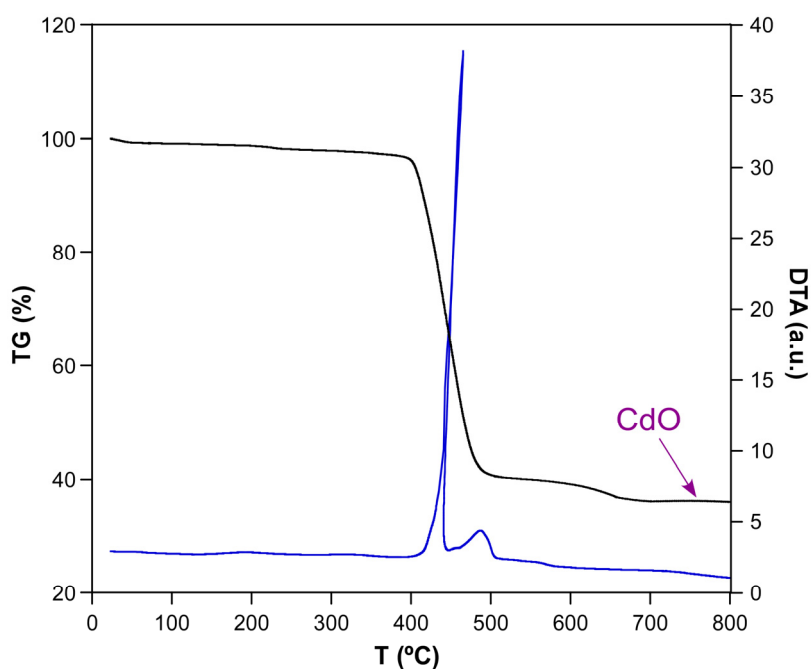


Figure S6. TG/DTA analysis for compound **1**.

S7. FT-IR spectroscopy.

FTIR spectrum of **1** has been assigned according to bibliography and the frequency modes derived from a DFT-optimized model of the compound (see Figure S12). At high frequencies, spectrum of **1** exhibits an intense band at 3470 cm^{-1} that corresponds to the vibration of the O–H bond of free water of moisture, followed by strong vibrations at 3330 and 3230 cm^{-1} related with N–H vibrations of the exocyclic amino group. Weak shoulders between 3100 and 2900 cm^{-1} are attributed to C–H vibrations of the pyridinic ring of the ligand. The intense vibrations in the 1670 – 1520 cm^{-1} region correspond to both the asymmetric stretching vibrations of the carboxylate groups and the aromatic C–C and C–N bonds, while the symmetric stretching vibrations of the carboxylate groups occur in the lower range of 1410 – 1270 cm^{-1} . At lower frequencies, the remaining bands are assigned to the distortions originated in the aromatic ring and the carboxylate groups of the 6ani ligand. The vibration bands of the Cd–O and Cd–N bonds are observed around 560 – 530 cm^{-1} .

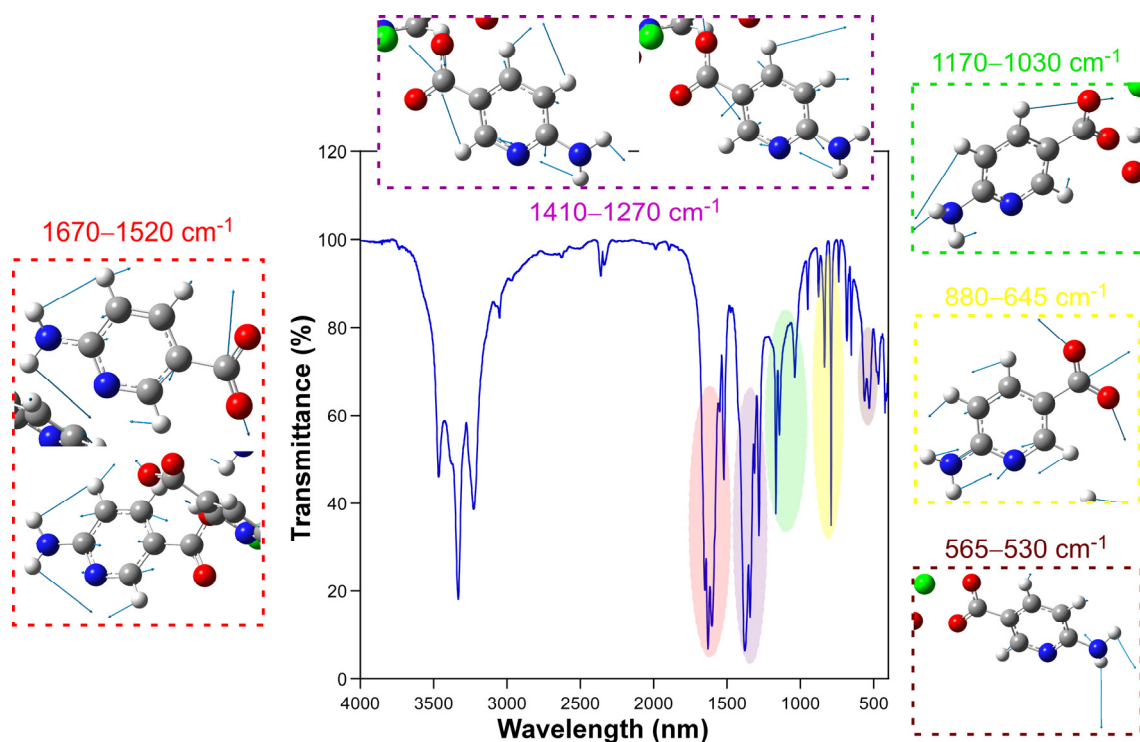


Figure S7. FTIR spectrum of compound **1** together with the normal vibration modes.

S8. Lifetime measurements.

Lifetime measurements were initially performed at 10 K using polycrystalline sample of **1** under excitation at the maximum (332 nm) for selected emission wavelengths in the 350–650 nm range. The decay curves were recorded employing different exposure times in order to achieve 10^4 counts in the pulse of reference. Given the different nature of the emissions (fluorescence below 410 nm and phosphorescence in the 410–600 nm range), nanosecond or microsecond pulse lamps were employed when appropriate. On the one hand, fitting result corresponding to the decay curve of the emission at 397 nm was obtained by deconvoluting the pulse signal according to the Instrument Response Function (IRF) at the same working conditions. On the other hand, eleven decay curves were recorded in the 410–600 nm range (one each *ca.* 20 nm) and analyzed by tail fitting (Figure S8-10). Most of decays were fitted using three parameters in order to reproduce fairly the non-linear curve, except for the first and last curves which are clearly less affected by the long-lasting phosphorescent emission.

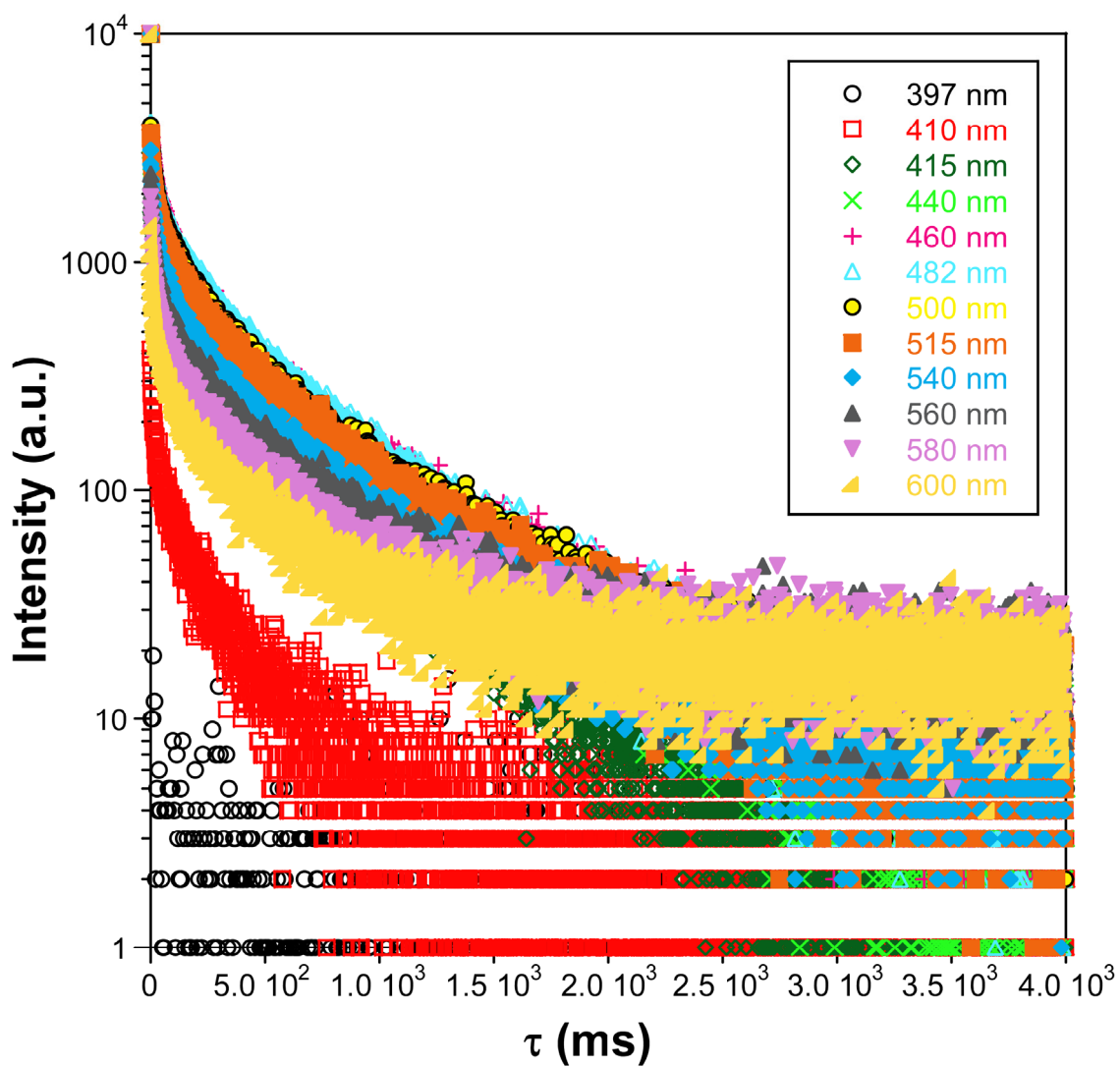


Figure S8. Decay curves at selected emission wavelengths upon excitation at 333 nm.

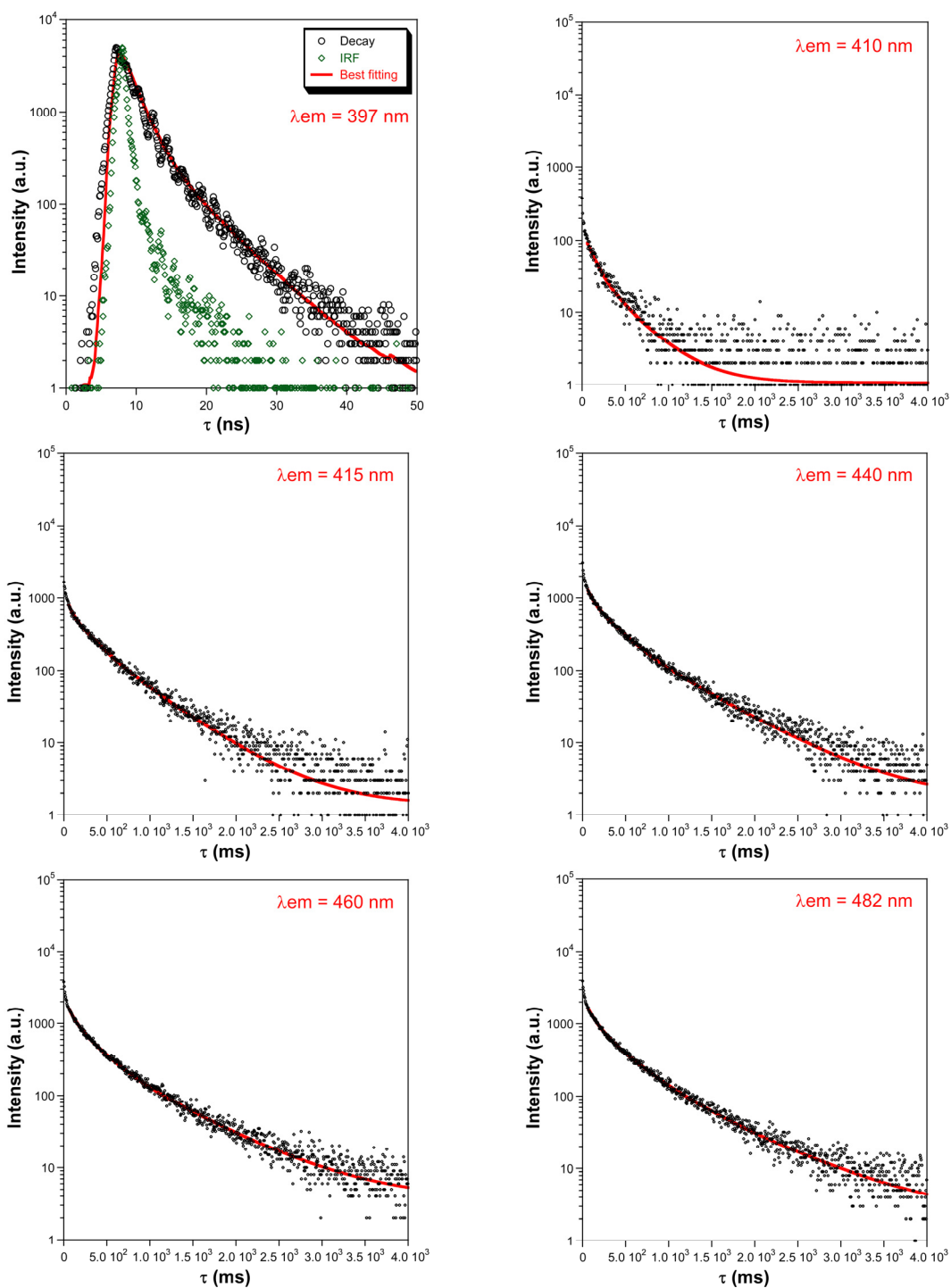


Figure S9. Emission decay curves at selected emission wavelength (at 397 nm and every *ca.* 20 nm in the 410–490 nm range) showing the best fitting.

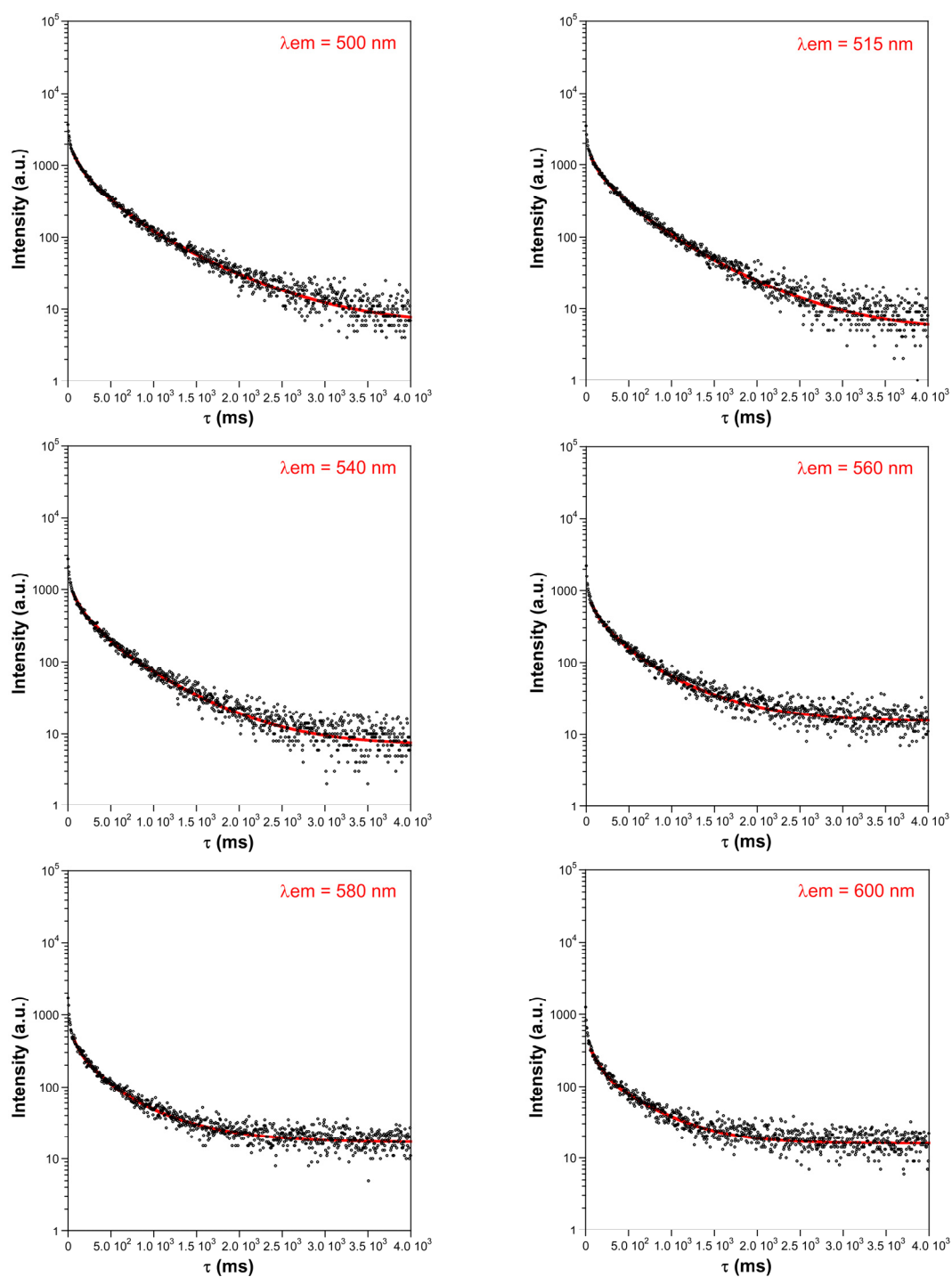


Figure S10. Emission decay curves at selected emission wavelength (every *ca.* 20 nm in the 500–600 nm range) showing the best fitting.

Table S5. Best fit results of decay curves performed at 10K monitoring emission wavelengths on the maxima.

Wavelength (nm)	τ_1 (ns)	Chi Sq.
397	5.9(1)	1.624

Table S6. Best fit results of decay curves performed at 10K monitoring different emission wavelengths.

Wavelength (nm)	τ_1 (ms)	τ_2 (ms)	τ_3 (ms)	Chi Sq.
410	113(8) / 33%	364(15) / 67%		1.286
415.65	58(8) / 4%	243(18) / 34%	557(15) / 62%	1.494
444	59(7) / 3%	246(10) / 38%	675(12) / 58%	1.510
460	62(5) / 4%	253(9) / 41%	718(14) / 55%	1.472
482	98(6) / 10%	340(18) / 49%	828(42) / 41%	1.494
500	77(5) / 8%	278(14) / 41%	737(22) / 51%	1.432
515	84(7) / 8%	295(21) / 41%	702(28) / 51%	1.493
540	60(6) / 9%	223(18) / 38%	629(21) / 53%	1.542
560	72(9) / 7%	260(29) / 37%	660(39) / 56%	1.452
580	60(9) / 6%	237(30) / 36%	624(40) / 58%	1.436
600	102(5) / 19%	489(8) / 81%		1.540

Additionally, variable-temperature measurements were performed at 444 and 482 nm emission peaks (maximum of the continuous spectrum and most long-lived emission, respectively). As shown in Table S7, the longest lifetime decreases slowly with rising the temperature.

Table S7. Best fit results of decay curves according to the temperature.

Temp. (K)	Wav. (nm)	τ_1 (ms)	τ_2 (ms)	τ_3 (ms)	Chi Sq.
10	444	59(7) / 3%	246(10) / 38%	675(12) / 58%	1.510
	482	98(6) / 10%	340(18) / 49%	828(42) / 41%	1.494
	515	84(7) / 8%	295(21) / 41%	702(28) / 51%	1.493
50	444	19(1) / 8%	96(4) / 28%	426(8) / 64%	1.447
	482	33(2) / 4%	166(16) / 18%	505(18) / 78%	1.392
	515	18(1) / 7%	114(7) / 25%	473(13) / 68%	1.547
100	444	14(1) / 6%	92(5) / 29%	371(11) / 65%	1.530
	482	14(1) / 2%	107(3) / 27%	430(6) / 71%	1.451
	515	15(1) / 2%	99(4) / 22%	422(5) / 75%	1.398
150	444	–	–	–	–
	482	22(3) / 4%	92(6) / 19%	422(7) / 77%	1.540
	515	21(2) / 4%	104(6) / 20%	428(7) / 76%	1.465
200	444	–	–	–	–
	482	31(2) / 6%	345(2) / 94%	–	1.568
	515	11(1) / 2%	60(5) / 9%	361(3) / 89%	1.514
250	444	–	–	–	–
	482	37(4) / 5%	300(3) / 95%	–	1.563
	515	19(2) / 2%	112(12) / 15%	294(8) / 83%	1.640

$\lambda_{em} = 444 \text{ nm}$ $\lambda_{em} = 482 \text{ nm}$ $\lambda_{em} = 515 \text{ nm}$

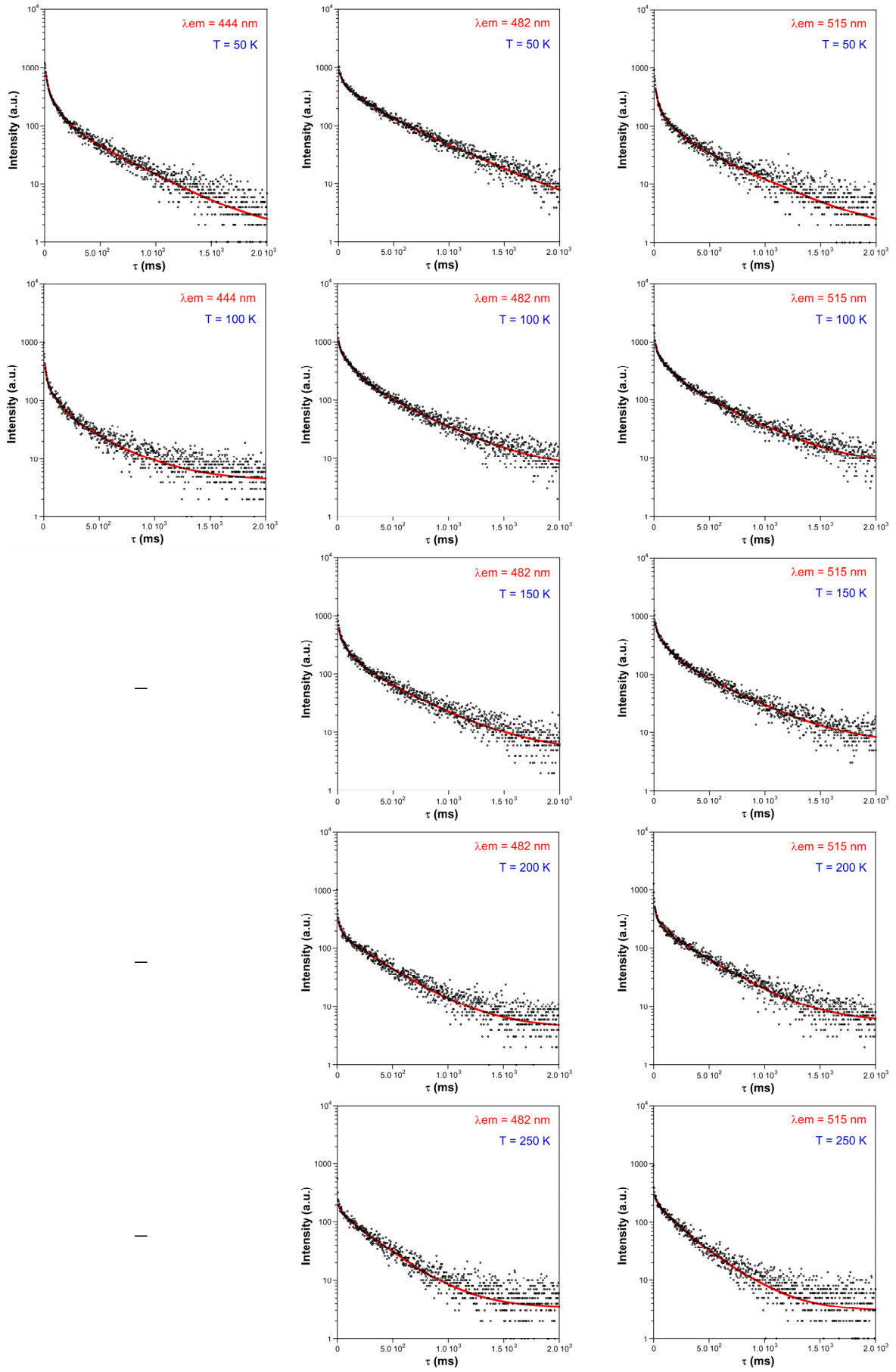


Figure S11. Variable-temperature decay curves fittings at selected emission lines.

S9. TD-DFT computational details.

TD-DFT theoretical calculations were performed at 10 K using the Gaussian 09 package.^{vii} Despite the Coulomb attenuating method- CAM-B3LYP functional^{viii} is said to describe reasonably well long-range charge transfer excitations, lately, several examples have been reported where the said functional did not fulfil expectations.^{ix} On the contrary, the use of the Becke three parameter hybrid functional with the non-local correlation functional of Lee-Yang-Parr (B3LYP)^x with the 6-31G(d)^{xi} basis set for all atoms but for the central metal cation which is described by the LANL2DZ^{xii} basis set along with the corresponding effective core potential (ECP), was proven to be highly reliable in describing the photophysics of the related zinc compound reported by our group previously.ⁱ In addition, the latter functional + basis set scheme has been proven to be an adequate method to describe luminescence of cadmium based coordination compounds.^{xiii} A suitable model of **1** (model **1** hereafter, Figure S12) was built from a cluster cut from the periodic structure optimized on the basis of the X-ray single crystal structure of the zinc counterpart (geometrically relaxed to adapt it to the cadmium atom, as detailed in section S4). Model **1** consists of an excerpt containing a cadmium atom coordinated to four 6ani ligands whose donor atoms establish the first coordination sphere of the metal. For the absorption and emission spectra, the 40 lowest singlet optical transitions were calculated on model **1** by the TD-DFT method (Tables S8–9). Vibronic progression of the modelled compound was neglected. Gaussian results were analyzed using the GaussSum program package^{xiv} and molecular orbitals plotted using GaussView 5.^{xv}

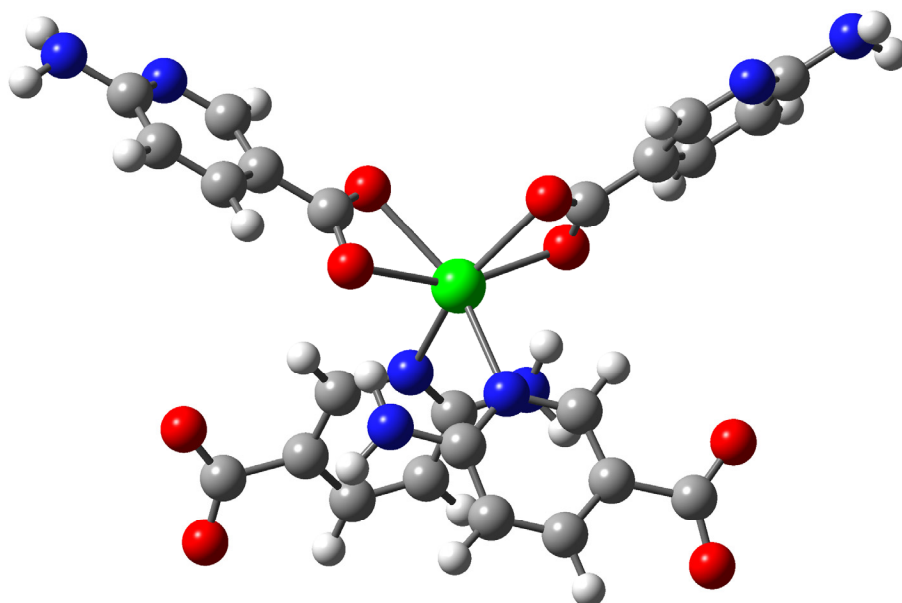
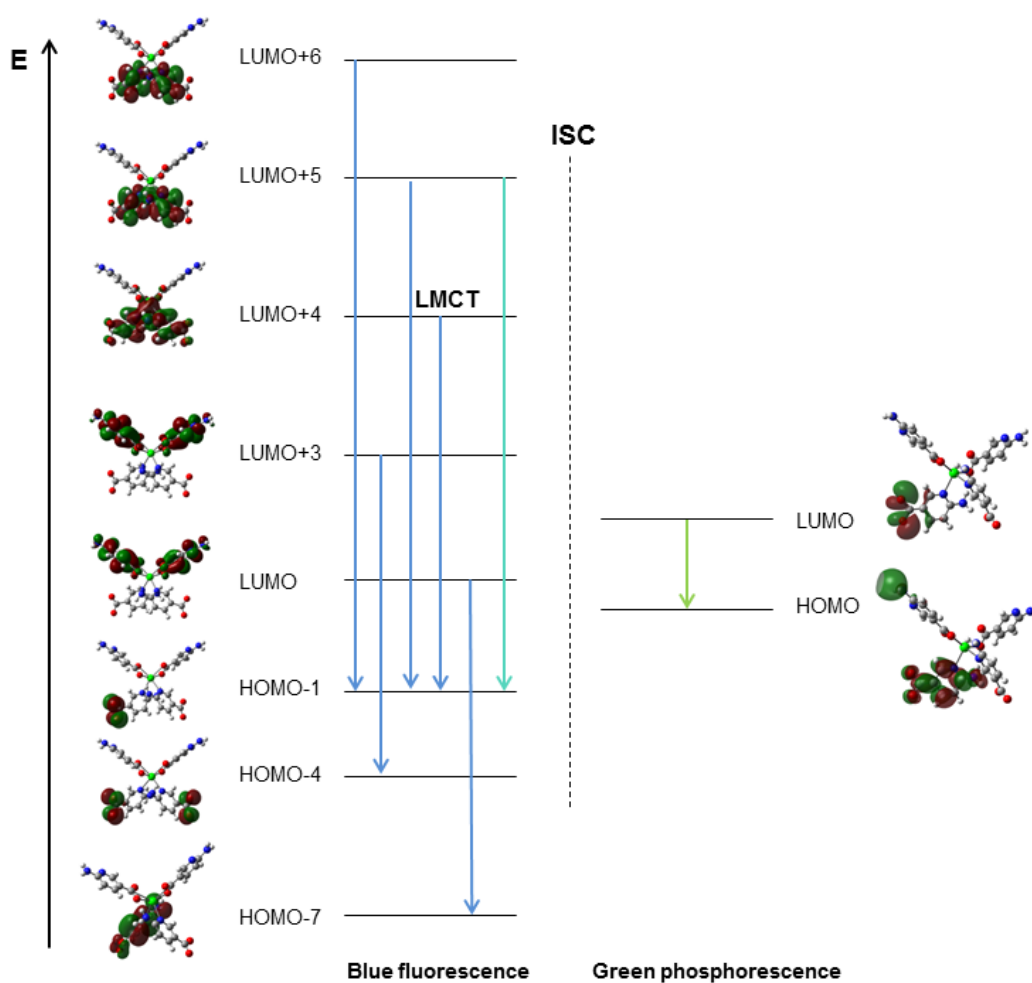


Figure S12. Molecular excerpt used as model **1** for the calculations.



Scheme S1. Energy diagram of the orbitals involved in the electronic transitions resulting in fluorescent (left) and phosphorescent (right) emissions of model **1**. ISC: Intersystem crossing; LMCT (Ligand to metal charge transfer).

Table S8. Calculated main excitation energies (nm) and singlet electronic transitions and associated oscillator strengths of model **1** in gas phase.

Calcd. λ (nm)	Exp. λ (nm)	Significant contributions	Osc. strength (a.u.)
344	332	HOMO \rightarrow LUMO + 6 (46%) HOMO - 1 \rightarrow LUMO + 7 (41%) HOMO - 5 \rightarrow LUMO + 4 (5%)	0.267
350	354	HOMO - 5 \rightarrow LUMO + 4 (59%) HOMO - 4 \rightarrow LUMO + 5 (30%) HOMO \rightarrow LUMO + 6 (4%)	0.234
375	372	HOMO - 2 \rightarrow LUMO + 4 (62%) HOMO - 3 \rightarrow LUMO + 5 (35%)	0.114
398	399	HOMO \rightarrow LUMO + 4 (65%) HOMO - 1 \rightarrow LUMO + 5 (35%)	0.021

Table S9. Calculated main emission energies (nm) and singlet electronic transitions and associated oscillator strengths of model **1** in gas phase.

Calcd. λ (nm)	Exp. λ (nm)	Significant contributions	Osc. strength (a.u.)
383	397	HOMO - 1 \leftarrow LUMO + 6 (96%)	0.106
394	397	HOMO - 4 \leftarrow LUMO + 3 (26%) HOMO - 5 \leftarrow LUMO + 3 (21%) HOMO - 1 \leftarrow LUMO + 9 (17%) HOMO - 4 \leftarrow LUMO + 5 (16%)	0.287
413	415	HOMO - 1 \leftarrow LUMO + 5 (99%)	0.483
443	444	HOMO - 1 \leftarrow LUMO + 5 (99%)	0.454
465	459	HOMO - 1 \leftarrow LUMO + 4 (85%) HOMO \leftarrow LUMO + 4 (9%)	0.379
467	459	HOMO - 7 \leftarrow LUMO (99%)	0.358
479	482	HOMO - 1 \leftarrow LUMO + 4 (91%) HOMO \leftarrow LUMO + 4 (8%)	0.316
497	515	HOMO - 1 \leftarrow LUMO + 5 (68%) HOMO \leftarrow LUMO + 4 (25%)	0.223

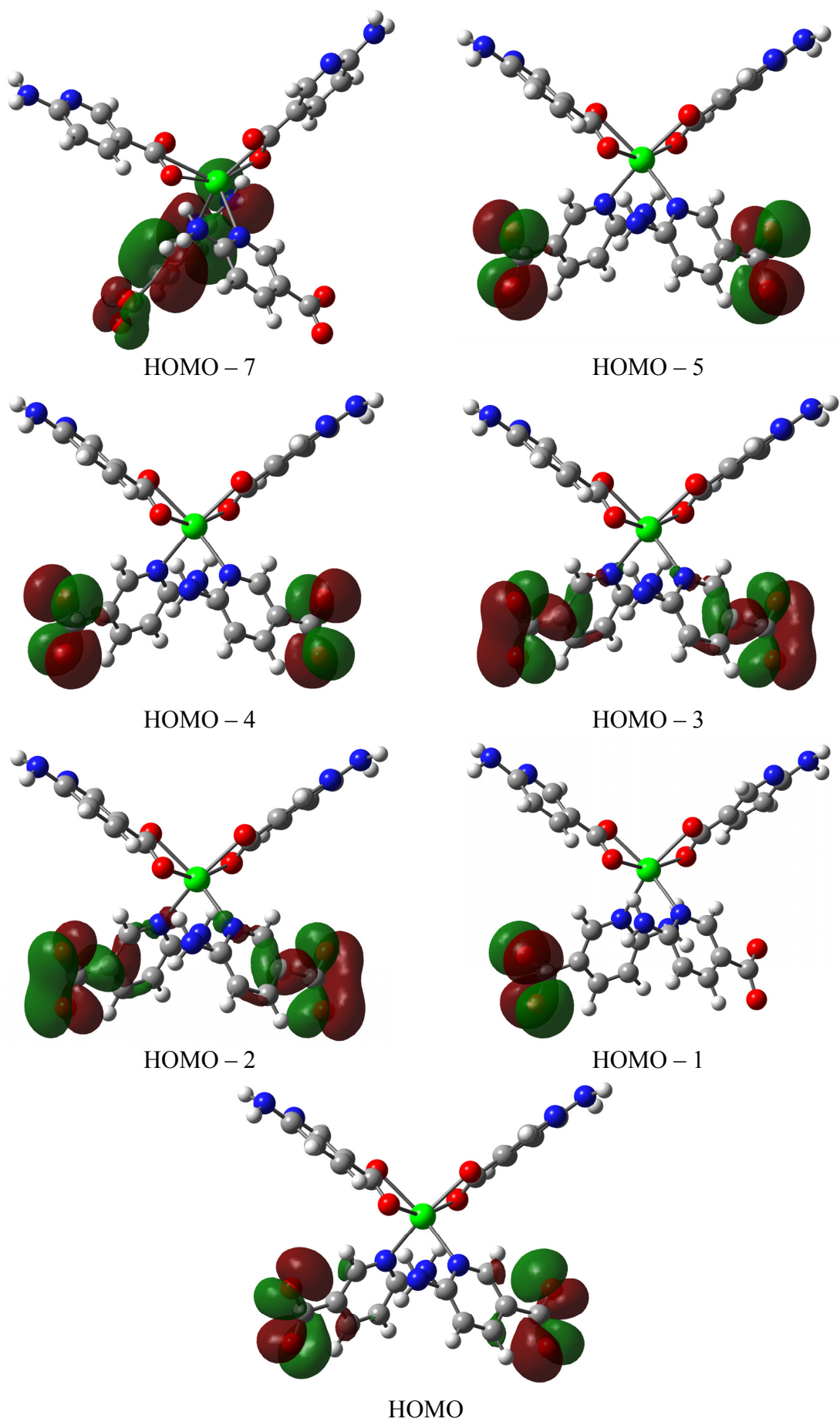


Figure S13. Highly Occupied Molecular Orbitals of model **1** involved in the singlet luminescent charge transitions.

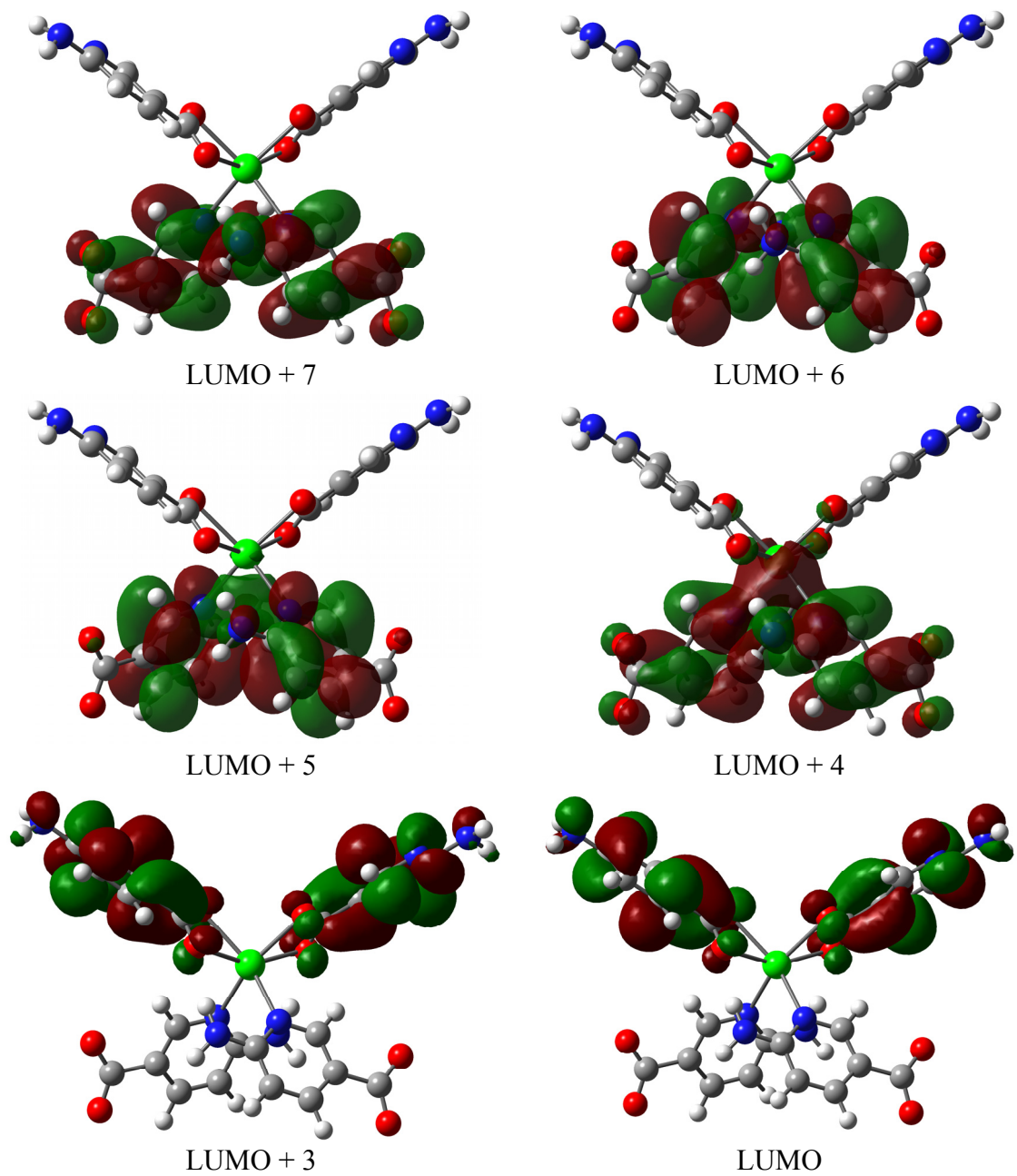


Figure S14. Lowest Unoccupied Molecular Orbitals of model **1** involved in the singlet luminescent charge transitions.

S10. Calculation of the lowest-lying triplet state (T_1).

The T_1-S_0 energy difference, which corresponds to the main phosphorescent emission line, has been estimated from vertical excitation performed for the optimised geometry of the lowest lying excited triplet state (T_1). The triplet state geometry optimisation and frequencies calculation was performed on a suitable model of **1** (Figure S15) by Gaussian 09 package, using the Becke three parameter hybrid functional with the non-local correlation functional of Lee-Yang-Parr (B3LYP) with the 6-31G++(d,p) basis set for all non-metal atoms and the LANL2DZ basis set along with the corresponding effective core potential (ECP) for the central cadmium cation.

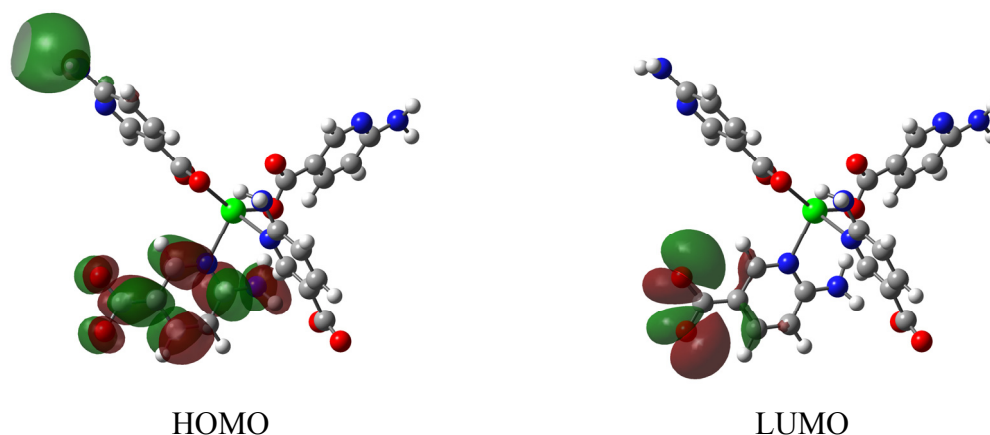


Figure S15. Highest Occupied (single-occupied alpha) and Lowest Unoccupied Molecular Orbitals of the first excited triplet state of model **1**.

The equivalent calculation was also performed on a suitable model of the previously reported isostructural Zn counterpartⁱ in order to estimate the T_1-S_0 energy difference. It was found that the calculated energy achieved matches fairly well that experimentally calculated. Figure S16 shows the corresponding optimised T_1 state geometry.

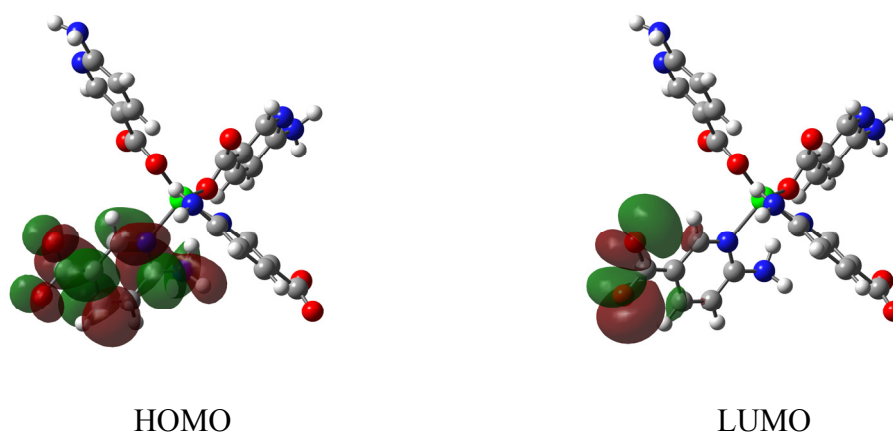


Figure S16. Highest Occupied (single-occupied alpha) and Lowest Unoccupied Molecular Orbitals of the first excited triplet state of model **1**.

S11. Time-resolved emission spectra.

TRES measurement was performed for the whole emission spectrum with a step size of 10 nm in the 400–650 nm range given the low emission of the material out of this range. The experiment was performed using a 0.5 Hz of frequency at the pulsed lamp, fixing the excitation band pass at 5 nm and the emission band pass at 2.5 nm. Each spectrum has been deconvoluted according to the standard colour system and plotted in the chromaticity CIE 1931 diagram.

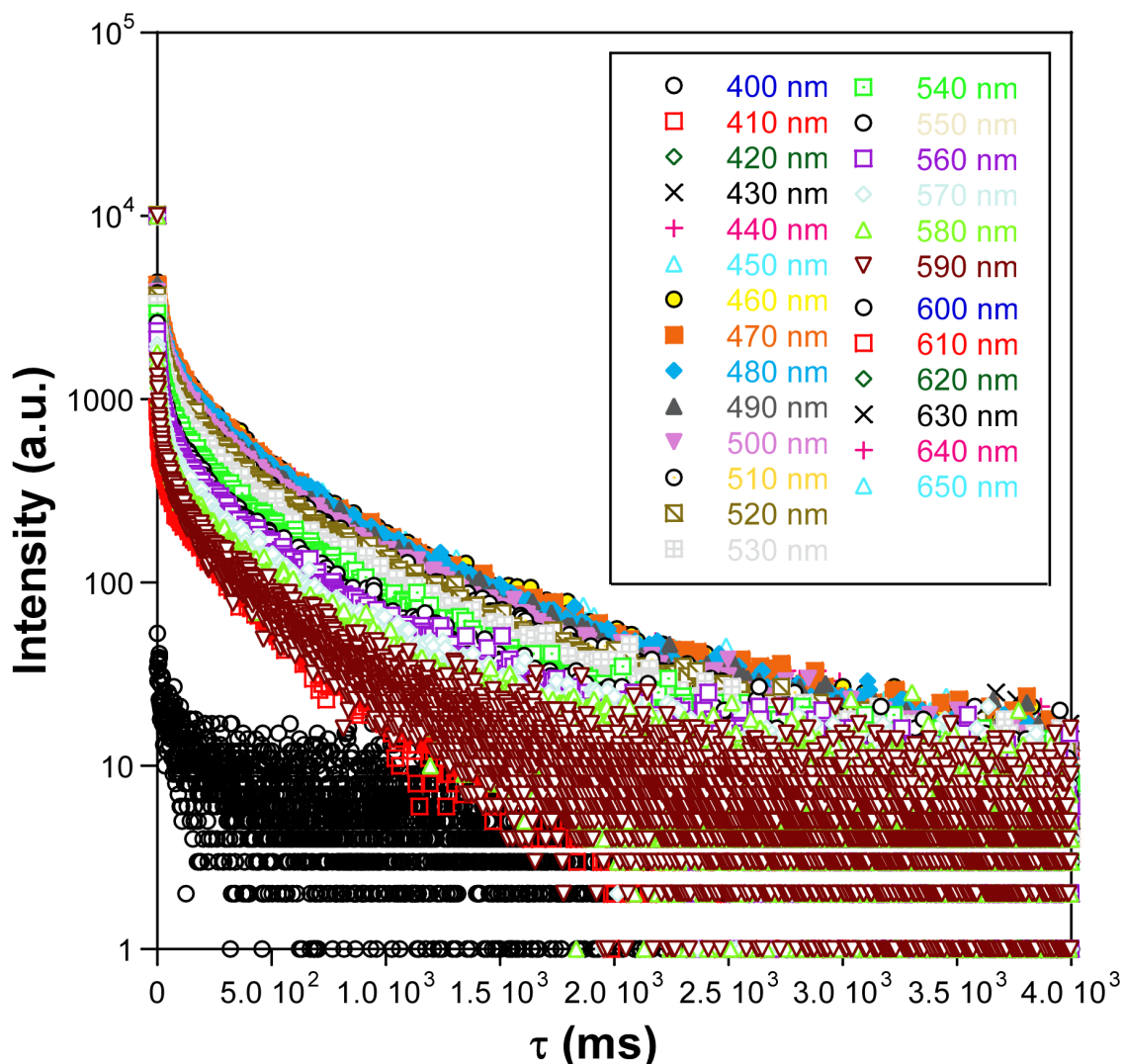


Figure S17. Time-resolved emission spectra in the 350–650 nm region.

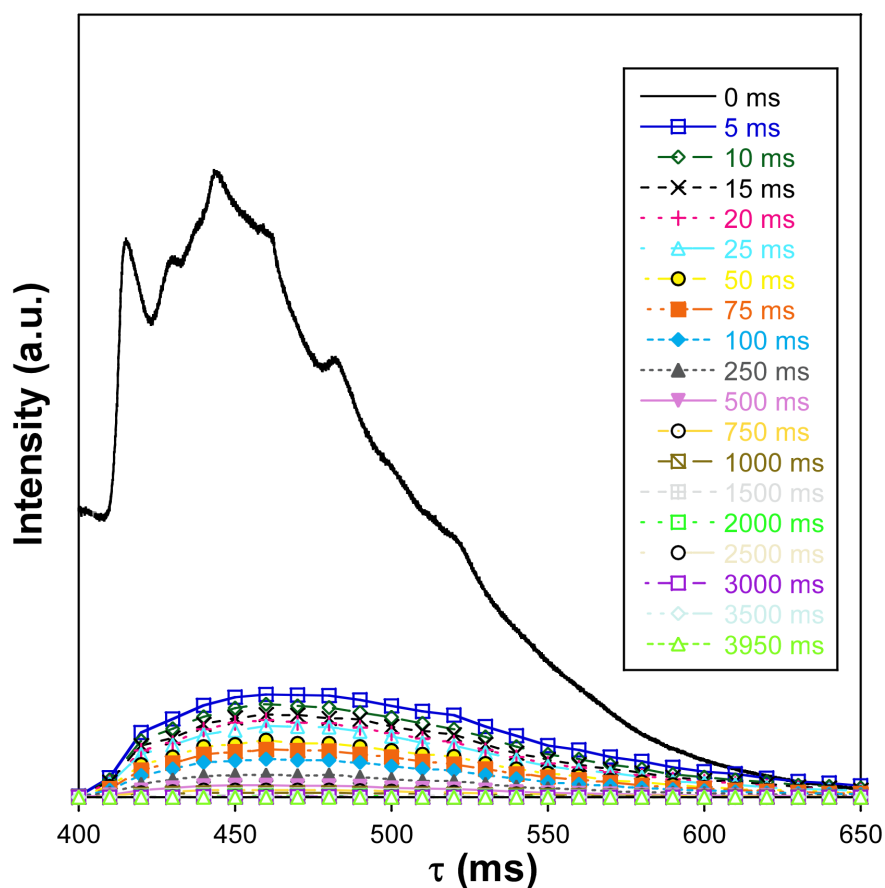


Figure S18. Time-resolved emission spectra at 10 K of **1** at different delays ($\lambda_{\text{ex}} = 333 \text{ nm}$).

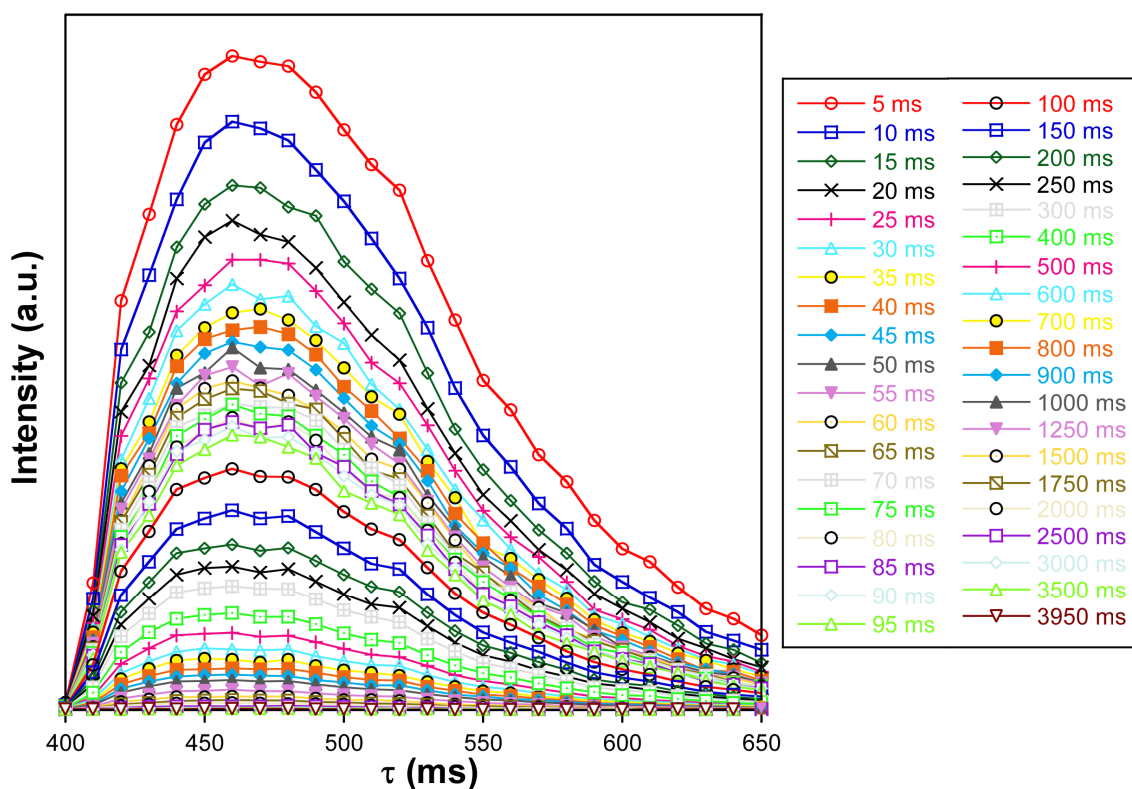


Figure S19. Detailed time-resolved emission spectra at 10 K of **1** at different delays ($\lambda_{\text{ex}} = 333 \text{ nm}$).

S12. References.

- ⁱ Cepeda, J.; San Sebastian, E.; Padro, D.; Rodríguez-Diéguez, A.; García, J. A.; Ugalde, J. M.; Seco, J. M. A Zn based coordination polymer exhibiting long-lasting phosphorescence. *Chem. Commun.* **2016**, *52*, 8671–8674.
- ⁱⁱ Soler, J. M.; Artacho, E.; Gale, J. D.; Garcia, A.; Junquera, J.; Ordejon, P.; Sanchez-Portal, D. The SIESTA method for ab initio order-N materials simulation. *J. Phys.: Condens. Matter* **2002**, *14*, 2745–2779.
- ⁱⁱⁱ (a) Baburin, I. A.; Leoni, S.; Seifert, G. Enumeration of Not-Yet-Synthesized Zeolitic Zinc Imidazolate MOF Networks: A Topological and DFT Approach. *J. Phys. Chem.* **2008**, *112*, 9437–9443. (b) Harvey, H. G.; Slater, B.; Attfield, M. P. Rational design of the pore system within the framework aluminium alkylendiphosphonate series. *Chem.–Eur. J.* **2004**, *10*, 3270–3278. (c) Lee, C.; Mellot-Draznieks, C.; Slater, B.; Wu, G.; Harrison, W. T. A.; Rao, C. N. R.; Cheetham, A. K. Thermodynamic and kinetic factors in the hydrothermal synthesis of hybrid frameworks: zinc 4-cyclohexene-1,2-dicarboxylates. *Chem. Commun.* **2006**, 2687–2649.
- ^{iv} Perdew, J. P.; Burke, K.; Ernzerhof, M. Generalized Gradient Approximation Made Simple. *Phys. Rev. Lett.* **1996**, *77*, 3865–3868.
- ^v <http://www.icmab.es/siesta/> (accessed on December 15, 2016).
- ^{vi} (a) Cepeda, J.; Pérez-Yáñez, S.; Beobide, G.; Castillo, O.; Fischer, M.; Luque, A.; Wright, P. A. Porous M^{II}/Pyrimidine-4,6-Dicarboxylate Neutral Frameworks: Synthetic Influence on the Adsorption Capacity and Evaluation of CO₂-Adsorbent Interactions. *Chem. Eur. J.* **2014**, *20*, 1554–1568. (b) Cepeda, J.; Pérez-Yáñez, S.; Beobide, G.; Castillo, O.; Goikolea, E.; Aguesse, F.; Garrido, L.; Luque, A.; Wright, P. A. Scandium/Alkaline Metal–Organic Frameworks: Adsorptive Properties and Ionic Conductivity. *Chem. Mater.* **2016**, *28*, 2519–2528.
- ^{vii} Frisch, M. J.; Trucks, G. W.; Schlegel, H. B.; Scuseria, G. E.; Robb, M. A.; Cheeseman, J. R.; Scalmani, G.; Barone, V.; Mennucci, B.; Petersson, G. A.; Nakatsuji, H.; Caricato, M.; Li, X.; Hratchian, H. P.; Izmaylov, A. F.; Bloino, J.; Zheng, G.; Sonnenberg, J. L.; Hada, M.; Ehara, M.; Toyota, K.; Fukuda, R.; Hasegawa, J.; Ishida, M.; Nakajima, T.; Honda, Y.; Kitao, O.; Nakai, H.; Vreven, T.; Montgomery Jr., J. A.; Peralta, J. E.; Ogliaro, F.; Bearpark, M.; Heyd, J. J.; Brothers, E.; Kudin, K. N.; Staroverov, V. N.; Kobayashi, R.; Normand, J.; Raghavachari, K.; Rendell, A.; Burant, J. C.; Iyengar, S. S.; Tomasi, J.; Cossi, M.; Rega, N.; Millam, J. M.; Klene, M.; Knox, J. E.; Cross, J. B.; Bakken, V.; Adamo, C.; Jaramillo, J.; Gomperts, R.; Stratmann, R. E.; Yazyev, O.; Austin, A. J.; Cammi, R.; Pomelli, C.; Ochterski, J. W.; Martin, R. L.; Morokuma, K.; Zakrzewski, V. G.; Voth, G. A.; Salvador, P.; Dannenberg, J. J.; Dapprich, S.; Daniels, A. D.; Farkas, O.; Foresman, J. B.; Ortiz, J. V.; Cioslowski, J. Fox, D. J. Gaussian 09, revision A.02, Gaussian, Inc., Wallingford, CT, 2009.
- ^{viii} Yanai, T.; Tew, D.; Handy, N. A new hybrid exchange–correlation functional using the Coulomb-attenuating method (CAM-B3LYP). *Chem. Phys. Lett.* **2004**, *393*, 51–57.
- ^{ix} (a) Humbert-Droz, M.; Pigué, C.; Wesolowski, T. A. Fluorescence quantum yield rationalized by the magnitude of the charge transfer in π -conjugated terpyridine derivatives. *Phys. Chem. Chem. Phys.* **2016**, *18*, 29387–29394. (b) Eriksen, J. J.; Sauer, S. P. A.; Mikkelsen, K. V.; Christiansen, O.; Jensen, H. J.; Kongsted, J. Failures of TDDFT in describing the lowest intramolecular charge-transfer excitation in para-nitroaniline. *Mol. Phys.* **2013**, *111*, 1235–1248.
- ^x (a) Becke, A. D. Density-functional thermochemistry. III. The role of exact exchange. *J. Chem. Phys.* **1993**, *98*, 5648–5652. (b) Miehlich, B.; Savin, A.; Stoll, H.; Preuss, H. Results obtained with the correlation energy density functionals of Becke and Lee, Yang and Parr. *Chem. Phys. Lett.* **1989**, *157*, 200–206. (c) Lee, C.; Yang, W.; Parr, R. G. Development of the Colle-Salvetti correlation-energy formula into a functional of the electron density. *Phys. Rev. B* **1988**, *37*, 785–789.
- ^{xi} (a) Rassolov, V. A.; Ratner, M. A.; Pople, J. A.; Redfern, P. C.; Curtiss, L. A. 6-31G* basis set for third-row atoms. *J. Comput. Chem.* **2001**, *22*, 976–984. (b) Francl, M. M.; Pietro, W. J.; Hehre, W. J.; Binkley, J. S.; DeFrees, D. J.; Pople, J. A.; Gordon, M. S. Self-consistent molecular orbital methods. XXIII. A polarization-type basis set for second-row elements. *J. Chem. Phys.* **1982**, *77*, 3654–3665. (c) Hariharan, P. C.; Pople, J. A. Accuracy of AH_n equilibrium geometries by single determinant molecular orbital theory. *Mol. Phys.* **1974**, *27*, 209–214.
- ^{xii} (a) Hay, P. J.; Wadt, W. R. Ab initio effective core potentials for molecular calculations. Potentials for the transition metal atoms Sc to Hg. *J. Chem. Phys.* **1985**, *82*, 270–283. (b) Wadt, W. R.; Hay, P. J. Ab initio effective core potentials for molecular calculations. Potentials for main group elements Na to Bi. *J. Chem. Phys.* **1985**, *82*, 284–298. (c) Hay, P. J.; Wadt, W. R. Ab initio effective core potentials for molecular calculations. Potentials for K to Au including the outermost core orbitals. *J. Chem. Phys.* **1985**, *82*, 299–310.

-
- ^{xiii} (a) Xu, H.; Huang, L.-F.; Guo, L.-M.; Zhang, Y.-G.; Ren, X.-M.; Song, Y.; Xie, J. Three green luminescent cadmium complexes containing 8-aminoquinoline ligands: Syntheses, crystal structures, emission spectra and DFT calculations. *J. Lumin.* **2008**, *128*, 1665–1672. (b) Wen, L.; Ke, X.; Qiu, L.; Zou, Y.; Zhou, L.; Zhao, J.; Li, D. Assembly of Two Porous Cadmium(II) Frameworks: Selective Adsorption and Luminescent Property. *Cryst. Growth Des.* **2012**, *12*, 4083–4089. (c) Wilbraham, L.; Coudert, F.-X.; Ciofini, I. Modelling photophysical properties of metal–organic frameworks: a density functional theory based approach. *Phys. Chem. Chem. Phys.* **2016**, *18*, 25176–25182.
- ^{xiv} O’Boyle, N. M.; Tenderholt, A. L.; Langner, K. M. cclib: A library for package-independent computational chemistry algorithms. *J. Comput. Chem.* **2008**, *29*, 839–845.
- ^{xv} GaussView, Version 5, R. Dennington, Keith, T.; Millam, J. *Semichem Inc.*, Shawnee Mission, KS, 2009.